International Journal of Automation and Computing 16(2), April 2019, 150-162
DOI: 10.1007/s11633-018-1156-5

Motion-force Transmissibility Characteristic Analysis of a Redundantly Actuated and Overconstrained Parallel Machine

Hai-Qiang Zhang Hai-Rong Fang Bing-Shan Jiang

School of Mechanical, Electronic and Control Engineering, Beijing Jiaotong University, Beijing 100044, China

Abstract: This paper presents a novel 1T2R three degrees of freedom redundantly actuated and overconstrained 2$\underline{\text{P}}$RU-$\underline{\text{P}}$R$\underline{\text{P}}$S parallel machining head ($\underline{\text{P}}$ denotes the active prismatic joint), which can construct 5-axis hybrid machine to complete high speed freedom surface milling for large complex structural components in aerospace. Firstly, based on the screw theory, the mobility of the proposed parallel manipulator is briefly analysed. Secondly, the kinematic inverse position and the parasitic motion of the parallel manipulator are explicitly expressed. Furthermore, motion-force transmission performance evaluation indices are derived in detail via an alternative approach based on the screw theory. More importantly, a simple method for quickly solving the maximum virtual power coefficient is proposed, and the motion-force transmission performance evaluation index is greatly improved. To evaluate the kinematic performance, its workspace is calculated. With numerical examples, performance distribution atlases of the manipulator are depicted visually. The corresponding results illustrate that the proposed parallel manipulator has better orientation workspace and superior motion-force transmission performance than the 2PRU-PRS parallel manipulator, which proves the validity and applicability of applying this manipulator as a machining head.

Keywords: Redundantly actuated, overconstrained, parallel manipulator, motion-force transmission performance, workspace.

1 Introduction

Hybrid configuration equipment with five degrees of freedom has the characteristics of compact structure, large workspace, and at the same, high stiffness, low inertia, and high reconfigurable ability due to its combination of serial and parallel topological structure advantages, which has been widely utilized in the aerospace and automotive industry for specified structural freedom surface milling processing and aluminum structural components assembly operations such as Sprint Z3 spindle head[1], the well-known Tricept hybrid machine tool[2], Exechon hybrid machine tool[3]. Moreover, another extremely successful parallel manipulator is the well-known Delta manipulator[4] that can be commonly employed for efficient high-speed pick-and-place applications. In practical engineering applications, to expand the workspace of the lower mobility parallel manipulator (PM), a long stroke rail can be connected normally in series, and to further improve the orientation ability of the end effector, a two or three degrees of freedom rotating head can be attached to the moving platform, which can construct a multi-degree of freedom hybrid manipulator with large workspace or high orientation capability. In order to ensure the machine tool can accomplish the complex processing task requirements, usually the manipulator needs to demonstrate high orientation capability, high stiffness and precision characteristics. In such circumstances, the overconstrained PM, as a special lower mobility, came into being, which means a PM with common constraints or redundant constraint such that the branch chain exerts the constrained fore or constrained couple on the moving platform. It mainly consists of two categories, i.e., the passive overconstrained and active overconstrained PM. Moreover, the active overconstrainted PM is comprised of a redundancy actuation PM and a redundantly actuated and overconstrained PM. Some excellent studies[5–8] on overconstrained PMs have been conducted, and numerous facts have proved that such manipulators can effectively avoid the singularity, increase the workspace, improve the kinematics and dynamics performance of machine tools, and improve stiffness as well, which has attracted increasing attention in both academia and industry.

At present, the 1T2R configuration parallel kinematic machines (PKM) have been extensively and successfully applied to a five-axis hybrid machine tool to process large and complex structural components with freedom surface machining, and numerous examples show that they have a good application prospects in manufacturing industry[9]. Therefore, it is the innovative configuration of the 1T2R

Research Article
Manuscript received May 23, 2018; accepted August 23, 2018; published online October 17, 2018
Recommended by Associate Editor Xun Xu

PM that is the kernel of the hybrid machine tool. There is an abundance of research on the 1T2R configuration mechanism. Kong et al.[10, 11] divided the 1T2R PM into three categories including PU configuration, UP configuration and RPR configuration. Li et al.[12] pointed out that a class of one translational and two rotational degrees of freedom (DOFs) PM called [PP]S configuration, mainly including 3-PRS, 3-RPS, 3-RRS and 3-PPS. Wang et al.[13] presented the 3-PUU PM with rotational and translational coupling degrees of freedom; the difference between the proposed mechanism and the 3PRS PM is that the former has no spherical joint, but yet possesses much larger rotation angle and higher precision. Cui et al.[14] designed a 3RPS PM with compound spherical joint that can increase the rotation angle. Li et al.[15] proposed a novel over-constrained 2RPU&SPR PM, the degree of freedom was analyzed based on screw theory, and a kinematic inverse position and a Jacobian matrix were derived. Xie et al.[16] conducted performance comparison analysis including motion-force transmission performance, parasitic motion and orientation capability of 2PRU-PRS and 2PRU-UPR overconstrainted PM. Pashkevich et al.[17] demonstrated the overconstrained PM can effectively improve the stiffness characteristic.

For the PM, the numerical methods fail to illustrate the relationship between the performance indices and parallel manipulator configurations, and therefore to explore and make full advantage of the optimal kinematic performance, which will be an important guiding significance for the configuration synthesis and dimensional optimization. At present, the performance evaluations are mainly based on the algebraic eigenvalue of the Jacobian matrix[18–25] and the motion-force transmission performance index in terms of screw theory. Ball[26] first proposed the concept of a virtual coefficient. Yuan et al.[27] defined the transfer factor as the evaluation index to estimate the motion-force transformation capability of the manipulator afterwards. Much progress has been made in developing the motion-force transmission capability based on previous researchers. Sutherland and Roth[28] performed a standardization of the transformation factor, and proposed the transmission index. Tsai and Lee[29, 30] improved the transmission index (TI), and proposed a method for computing the maximum of the transfer rate and virtual coefficient, however, the final results relied on the selected reference point cannot reflect the inherent transmission performance of the PM. Takeda and Funabashi[31] defined a novel power transmission index for parallel manipulators based on the notion of pressure angles, and the minimum value of cosines of the pressure angles can be demonstrated with the motion transmissibility. Then, Chen and Angeles[32] proposed a generalized transmission index (GTI) and the virtual coefficient maximum value was modified, which are applied to evaluate the motion-force transmission performance of the single loop spatial linkage. Xie et al.[33, 34] proposed a new motion-force transmission performance system, and the calculation criteria of the output twist screw are systematically addressed in reachable position and orientation workspace, the input and output transmission index and local transmission index (LTI) and good transmission workspace (GTW) were defined based on the power transmission coefficients. Huang et al.[35, 36] constructed the mapping matrix which can describe the transformation relationship of force and motion between joint space and operation space by resorting to dual bases and dual space, and kinematic performance evaluation indices such that inter chain and intra chain transmission performance are deduced. Because the instantaneous virtual power and the maximum transmission power ratio is an important index with which to evaluate the motion-force characteristics, this method is more suitable for lower mobility PMs with the combined DOFs in terms of translations and rotations.

Undoubtedly, workspace is also a key performance index of PM, so it is necessary to investigate the workspace in more detail. Many scholars investigated this with different methods and algorithms. In [37, 38], a discrete boundary searching method was implemented to calculate the workspace of PM considering the driving and rotation angle constraints in the polar coordinate system. Pond and Carretero[39] investigated the reachable workspace and dexterous workspace of three PMs (including 3-PRS, 3-RPS, and Tricept) based on a homogeneous Jacobian matrix condition number, and conducted quantitative analysis on the workspace. Herrero et al.[40] solved the workspace of 2PRU-1PRS PM based on the calculation of inverse kinematics and geometrical constraint and singularity constraint. What′s more, they pointed out that maximum inscribed ball can be utilized to measure the workspace. Fu and Gao[41] obtained the position workspace and orientation workspace of the PM by using a numerical searching method, and determined the maximum inscribed cylinder and sphere envelope by parameter optimal design for a specified workspace.

A novel redundantly actuated and overconstrained 2$\underline{P}$RU-$\underline{P}$R$\underline{P}$S PM is proposed, which can be applied to high speed freedom surface machining for large complex components in the aerospace field. By resorting to screw of theory, the mobility of the PM was briefly analyzed. The closed-loop vector method is employed to establish the mathematical model of inverse kinematics; afterwards, the orientation conversion relations between the Euler angle and T-T angle are explicitly derived. The transmission performance indices are mathematically expressed by using the theory of reciprocal screws. A new and simple calculation method of potential maximum transmission power is straightforwardly deduced, and the maximum virtual power coefficient can be obtained expediently via this approach. To evaluate the kinematic performance, its workspace is calculated. With numerical examples, performance distribution atlases and workspace of the manipulator are depicted visually. Finally,

the performance indices are investigated and the comparisons are made, and some useful conclusions are given.

2 Mobility analysis of the parallel manipulator

2.1 Architecture description

A novel redundantly actuated and overconstrained 2PRU-PRPS PM (P denotes the active prismatic joint) has been proposed in this paper, as shown in Fig.1, which is composed of a moving platform, a fixed base and two identical constrained PRU chains and one double actuated PRPS chain together connecting the fixed base and the moving platform by a prismatic (P) joint, a revolute (R) joint followed by a universal (U) joint or a spherical (S) joint in sequence. Two of the PRU chains are symmetrically arranged and are located in a plane, furthermore two rotational axes are parallel to each other, the second revolute axes of two Hooke joints are coincident, and perpendicular to the third revolute axis of the spherical joint. The PM is actuated by four active prismatic joints, and three actuators are fixed at the base, which reduces the inertia of the parallel manipulator tool[42]. The spindle head is mounted at the end of the moving platform to accomplish the high speed milling.

For the purpose of facilitating analysis, as depicted in Fig. 2, fixed coordinate system B-xyz is located at the center of the fixed base, and a moving coordinate system A-uvw is attached at the center of the moving platform,

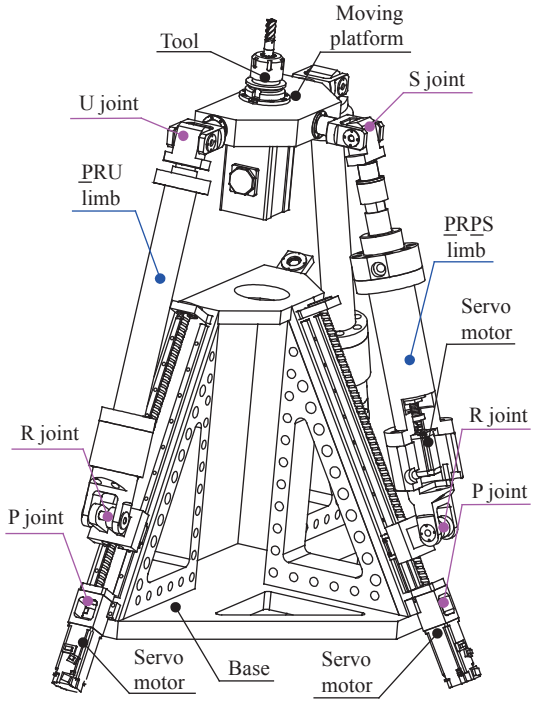

Fig. 1 3D model of the 2-PRU-PRPS PM (Color versions of the figures in this paper are available online)

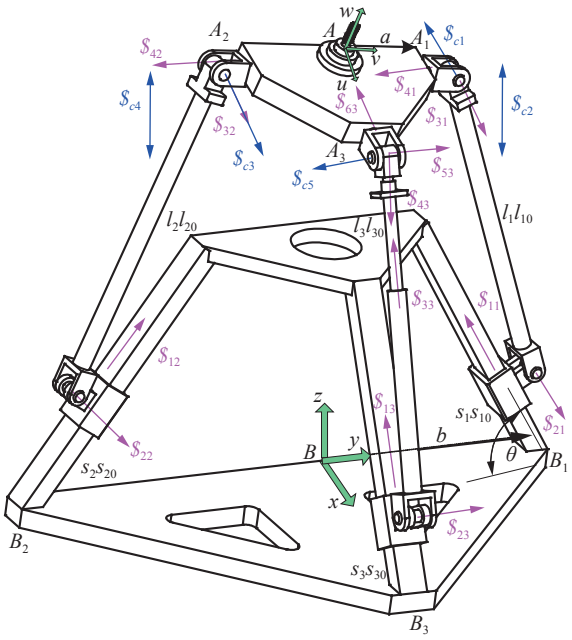

Fig. 2 Schematic diagram of the PM

respectively. Let the middle point of hypotenuse B_1B_2 be B, the x-axis is perpendicular to B_1B_2, the y-axis coincides with B_1B_2, and the z-axis is perpendicular to the fixed base upward. Similarly, let the middle point of hypotenuse A_1A_2 be A, the u-axis is perpendicular to A_1A_2, v-axis is coincide with A_1A_2, and the w-axis is perpendicular to the moving platform upward. Without loss of generality, $\Delta B_1B_2B_3$ and $\Delta A_1A_2A_3$ are both isosceles right triangles, $\angle B_1B_3B_2{=}\angle A_1A_3A_2{=}90^\circ$, and their circumradius are designated as a and b, respectively. $BB_1{=}BB_2{=}BB_3{=}b$, and $AA_1{=}AA_2{=}AA_3{=}a$. With respect to B-xyz, the position vector of B_1, B_2 and B_3 are $(0\ b\ 0)$, $(0\ -b\ 0)$, $(b\ 0\ 0)$, and A_1, A_2, and A_3 are $(x_1\ y_1\ z_1)$, $(x_2\ y_2\ z_2)$, $(x_3\ y_3\ z_3)$, respectively. The layout angle of the fixed actuators is defined as θ.

2.2 Mobility determination

The mobility determination is the first and foremost issue in designing a PM. In order to determine the motion pattern of the 2PRU-PRPS PM, mobility analysis is indispensable. Furthermore, it is necessary to analyze the constraint screw provided by each branched chain to the moving platform, and comprehensively analyze the constraint type of the moving platform, and the detailed analysis process is as follows.

The twist screw of the first PRU limb is given in the fixed coordinate system by

$$\begin{cases} \$_{11} = (0 \quad 0 \quad 0;\ 0 \quad -c\theta \quad s\theta) \\ \$_{21} = (1 \quad 0 \quad 0;\ 0 \quad s_1s\theta \quad s_1c\theta - b) \\ \$_{31} = (1 \quad 0 \quad 0;\ 0 \quad z_1 \quad -y_1) \\ \$_{41} = (0 \quad e_1 \quad f_1;\ f_1y_1 - e_1z_1 \quad -f_1x_1 \quad e_1x_1) \end{cases} \tag{1}$$

where s and c are the abbreviation of *sine* and *cosine*, respectively, s_i denotes the twist of the P joint, and e_i and f_i represent the direction cosine of the second revolute axis of the Hooke joint of i limb.

Then, employing reciprocal screw theory, the wrench system of (1) is easily obtained as

$$\begin{cases} \$_{c1} = (e_1 \quad 0 \quad 0;\ 0 \quad e_1z_1 - f_1y_1 \quad 0) \\ \$_{c2} = (0 \quad 0 \quad 0;\ 0 \quad -f_1 \quad e_1) \end{cases} \tag{2}$$

where $\$_{c1}$ represents a constraint force that passes through the point A_1 and is parallel to $\$_{21}$, and $\$_{c2}$ represents a constraint couple that is perpendicular to v and $\$_{31}$.

In a similar approach, the twist screw of the second PRU limb can be expressed mathematically as

$$\begin{cases} \$_{12} = (0 \quad 0 \quad 0;\ 0 \quad c\theta \quad s\theta) \\ \$_{22} = (1 \quad 0 \quad 0;\ s_2s\theta \quad 0 \quad b - s_2c\theta) \\ \$_{32} = (1 \quad 0 \quad 0;\ 0 \quad z_2 \quad -y_2) \\ \$_{24} = (0 \quad -e_1 \quad -f_1;\ e_1z_2 - f_1y_2 \quad f_1x_2 \quad -e_1x_2). \end{cases} \tag{3}$$

The wrench screw of (3) is obtained as

$$\begin{cases} \$_{c3} = (e_1 \quad 0 \quad 0;\ 0 \quad e_1z_2 - f_1y_2 \quad 0) \\ \$_{c4} = (0 \quad 0 \quad 0;\ 0 \quad -f_1 \quad e_1) \end{cases} \tag{4}$$

where $\$_{c3}$ represents a constraint force that passes through the point A_2 and is parallel to the $\$_{22}$, and $\$_{c4}$ represents a constraint couple that is perpendicular to v and $\$_{32}$.

The twist screw of the third PRPS limb can be expressed numerically as

$$\begin{cases} \$_{13} = (0 \quad 0 \quad 0;\ -c\theta \quad 0 \quad s\theta) \\ \$_{23} = (0 \quad 1 \quad 0;\ -s_3s\theta \quad 0 \quad b - s_3c\theta) \\ \$_{33} = (0 \quad 0 \quad 0;\ m_3 \quad 0 \quad n_3) \\ \$_{43} = (-m_3 \quad 0 \quad -n_3;\ -n_3y_3 \quad n_3x_3 - m_3z_3 \quad m_3y_3) \\ \$_{53} = (-n_3 \quad e_3 \quad m_3;\ m_3y_3 - e_3z_3 \quad -m_3x_3 - n_3z_3 \\ \qquad e_3x_3 + n_3y_3) \\ \$_{63} = (g_1 \quad -f_1 \quad e_1;\ e_1y_3 + f_1z_3 \quad g_1z_3 - e_1x_3 \\ \qquad -f_1x_3 - g_1y_3) \end{cases} \tag{5}$$

where $g_1 = \dfrac{e_1m_3 - f_1e_3}{n_3}$, e_3 is a constant, m_3 and n_3 represent the direction cosine of the third joint axis.

Subsequently, the wrench screw of (5) can be expressed as

$$\$_{c5} = (0 \quad 1 \quad 0;\ -z_3 \quad 0 \quad x_3) \tag{6}$$

where $\$_{c5}$ represents a constraint force that passes through the point A_3 and is parallel to the screw $\$_{23}$.

So far, the constraint wrench screw of the PM can be expressed as

$$\begin{cases} \$_{c1} = (e_1 \quad 0 \quad 0;\ 0 \quad e_1z_1 - f_1y_1 \quad 0) \\ \$_{c2} = (0 \quad 0 \quad 0;\ 0 \quad -f_1 \quad e_1) \\ \$_{c3} = (e_1 \quad 0 \quad 0;\ 0 \quad e_1z_2 - f_1y_2 \quad 0) \\ \$_{c4} = (0 \quad 0 \quad 0;\ 0 \quad -f_1 \quad e_1) \\ \$_{c5} = (0 \quad 1 \quad 0;\ -z_3 \quad 0 \quad x_3). \end{cases} \tag{7}$$

It should be noted that the direction vector A_1A_2 coincides with the second joint axis of the Hooke joint in the two PRU limbs, so the relation can be obtained as

$$\frac{z_2 - z_1}{y_2 - y_1} = \frac{f_1}{e_1}. \tag{8}$$

By combining (8) and rearranging (7), the twist screw of the moving platform yields the following:

$$\begin{cases} \$_1^m = (1 \quad 0 \quad 0;\ 0 \quad z_3 \quad 0) \\ \$_2^m = (0 \quad e_1 \quad f_1;\ f_1y_2 - e_1z_2 \quad 0 \quad 0) \\ \$_3^m = (0 \quad 0 \quad 0;\ 0 \quad 0 \quad 1). \end{cases} \tag{9}$$

In (9), $\$_1^m$ represents one rotational degree of freedom that passes through the point A_3 and is parallel to the x-axis, $\$_2^m$ represents one rotational degree of freedom of the moving platform that passes through the point A_2 and is parallel to the v-axis, and $\$_3^m$ represents a translational degree of freedom that is perpendicular to the fixed base. Note that the proposed manipulator has the same degree of freedom and kinematics characteristics compared with the 2PRU-PRS PM.

3 Kinematic analysis

3.1 Position inverse analysis

The inverse kinematics solution is based on the determination of the structural parameters of the mechanism, when the position and orientation of the moving platform are given, so as to solve the input displacement of the prismatic joints.

The position vector of the original point A in the fixed coordinate system $B - xyz$ can be denoted by $\boldsymbol{p} = \begin{bmatrix} x & y & z \end{bmatrix}^{\mathrm{T}}$. $\boldsymbol{a}_i$ and $\boldsymbol{b}_i$ represent the position vector of joint A_i and B_i in the fixed coordinate, which can be respectively expressed in matrix form as

$$\begin{cases} \boldsymbol{a}_1 = \boldsymbol{R}(0 \quad a \quad 0)^{\mathrm{T}} \\ \boldsymbol{a}_2 = \boldsymbol{R}(0 \quad -a \quad 0)^{\mathrm{T}}, \\ \boldsymbol{a}_3 = \boldsymbol{R}(a \quad 0 \quad 0)^{\mathrm{T}} \end{cases} \begin{cases} \boldsymbol{b}_1 = (0 \quad b \quad 0)^{\mathrm{T}} \\ \boldsymbol{b}_2 = (0 \quad -b \quad 0)^{\mathrm{T}} \\ \boldsymbol{b}_3 = (b \quad 0 \quad 0)^{\mathrm{T}} \end{cases} \tag{10}$$

where $\boldsymbol{R}$ denoted the orientation matrix, herein one adopted *Z-Y-X* Euler angles to describe the orientation matrix of the moving coordinate system with respect to the fixed coordinate system, first rotating the moving coordinate about the z-axis by angle γ, then about the y-axis of the new coordinate system by angle β, and finally

about the x-axis of the new coordinate system by angle α. Thus, this can be expressed as

$$\boldsymbol{R} = \boldsymbol{R}(\gamma, z)\,\boldsymbol{R}(\beta, y)\,\boldsymbol{R}(\alpha, x) = \begin{bmatrix} c\beta c\gamma & s\alpha s\beta c\gamma - c\alpha s\gamma & c\alpha s\beta c\gamma + s\alpha s\gamma \\ c\beta s\gamma & s\alpha s\beta s\gamma + c\alpha c\gamma & c\alpha s\beta s\gamma - s\alpha c\gamma \\ -s\beta & s\alpha c\beta & c\alpha c\beta \end{bmatrix}. \quad (11)$$

Because of the arrangement of the revolute joint, the center of Hooke joints and spherical joint cannot move along the axis of the revolute joint, so the following constraint conditions can be structured as

$$\begin{cases} (\boldsymbol{p} + \boldsymbol{a}_1)^{\mathrm{T}} \cdot (1 \quad 0 \quad 0) = 0 \\ (\boldsymbol{p} + \boldsymbol{a}_2)^{\mathrm{T}} \cdot (1 \quad 0 \quad 0) = 0 \\ (\boldsymbol{p} + \boldsymbol{a}_3)^{\mathrm{T}} \cdot (0 \quad 1 \quad 0) = 0. \end{cases} \quad (12)$$

Selecting parameters α, β and z as three independent parameters, parasitic motion can be arranged as

$$\begin{cases} x = 0 \\ y = -ac\beta s\gamma \\ \gamma = \arctan\left(\dfrac{s\alpha s\beta}{c\alpha}\right). \end{cases} \quad (13)$$

The close-loop vector method is used to establish the equation of vector A_iB_i in the fixed coordinate system B-xyz as the following:

$$\boldsymbol{L}_i = \boldsymbol{a}_i + \boldsymbol{p} - \boldsymbol{b}_i = l_i\boldsymbol{l}_{i0} + s_i\boldsymbol{s}_{i1}. \quad (14)$$

Taking the square of both sides of (14) yields

$$s_i^2 - 2\boldsymbol{L}_i^{\mathrm{T}} s_{i1} s_i + \boldsymbol{L}_i^{\mathrm{T}}\boldsymbol{L}_i - {l_i}^2 = 0. \quad (15)$$

Position inverse solution of the PM about s_i in (15) can be analysed in detail as follows, which is used to determine the reachable workspace of the manipulator[43].

$$s_i = \boldsymbol{L}_i^{\mathrm{T}} s_{i1} \pm \sqrt{\left(\boldsymbol{L}_i^{\mathrm{T}} s_{i1}\right)^2 - \boldsymbol{L}_i^{\mathrm{T}} \cdot \boldsymbol{L}_i + {l_i}^2} \quad (16)$$

where $s_{i1} = \begin{bmatrix} -c\theta_i c\theta & -s\theta_i c\theta & s\theta \end{bmatrix}^{\mathrm{T}}$, l_1=l_2=l, and l_3 is an extensible and compressible chain.

3.2 Orientation description of tilt-torsion (T-T) angle

To better describe the orientation capability of the PM, Liu et al.[44] pointed out that the [PP]S mechanism is three-degree of freedom with zero torsion angle, and systemically studied the relationships between different Euler angles and the tilt-torsion (T-T) angle, i.e., the orientation of the moving platform can be easily described as the azimuth angle and tilt angle. When the torsion angle is zero, the orientation matrix of T-T angle can be expressed as

$${}^{T-T}\boldsymbol{R}(\varphi, \phi, 0) = \boldsymbol{R}_z(\varphi)\,\boldsymbol{R}_y(\phi)\,\boldsymbol{R}_z(-\varphi)\,\boldsymbol{R}_z(0) = \begin{bmatrix} s^2\varphi + c^2\varphi c\phi & s\varphi c\phi(c\phi - 1) & c\varphi s\phi \\ s\varphi c\phi(c\phi - 1) & c^2\varphi + s^2\varphi c\phi & s\varphi s\phi \\ -c\varphi s\phi & -s\varphi c\phi & c\phi \end{bmatrix}. \quad (17)$$

Combining (11) and (17), the T-T angles with zero-torsion can be converted to the Z-Y-X Euler angles via the following equations:

$$\begin{cases} \beta = a\sin(c\varphi s\phi) \\ \alpha = a\sin\left(\dfrac{-s\varphi s\phi}{c\beta}\right) \\ \gamma = a\sin\left(\dfrac{s\varphi c\phi\,(c\phi - 1)}{c\beta}\right). \end{cases} \quad (18)$$

4 Motion-force transmission performance

4.1 Screw analysis

In practice, it is a kind of ability that power is mainly transmitted from the actuators to the moving platform. However, the power will be loss a lot in the transmission process. Therefore, we can treat the motion-force transmission capability as the performance index to measure the transmissibility of the PM.

In order to introduce the motion-force transmission performance index, a single chain is taken as an example to analyse the motion screw and the constraint screw $\$_{ck}$ of the chain is obtained by reciprocal product.

Since the prismatic joint of the PM is the active joint, so the corresponding motion screw denotes the input twist screw (ITS), which can be expressed as follows:

$$\$_{Ii} = \$_{1i} = (0 \quad 0 \quad 0;\ -c\theta_i c\theta \quad -s\theta_i c\theta \quad s\theta) \quad (19)$$

where θ_i denotes the angle between the joint B_i of the fixed base and the x-axis of the fixed coordinate system, here $\theta_1 = \dfrac{\pi}{2}$, $\theta_2 = -\dfrac{\pi}{2}$, and $\theta_3 = 0$.

Assume that the input twist screw is locked temporarily, a new unit transmission wrench screw (TWS) $\$_{Ti}$ can then be obtained, which represents the intermediate medium that transmit the power from the input to the output terminal.

$$\$_{Ti} = \left(\boldsymbol{l}_{i0}{}^{\mathrm{T}};\ (\boldsymbol{a}_i \times \boldsymbol{l}_{i0})^{\mathrm{T}}\right). \quad (20)$$

Obviously, the constraint wrench screw $\$_{Ti}$ denotes a pure force in the link direction passing through the point A_i.

When all the active prismatic joints except the i-th chain are locked, then the manipulator became the single degree of freedom for the time being. In this situation, only the unlocked transmission wrench represented by $\$_{Ti}$

can contribute to the moving platform, while all other transmission wrenches don't do any work. In other words, the three locked transmission wrenches can be treated as additional constraint wrenches at this time. Thereby, the instantaneous motion screw of the end effector was called the output twist screw (OTS), then for convenience of a further derivation, the output twist screw $\$_{Oi}$ can be expressed with six algebraic symbols:

$$\$_{Oi} = (l \quad m \quad n;\ d \quad e \quad f)\,. \tag{21}$$

Simultaneously, the output twist screw $\$_{Oi}$ should satisfy the following constraint conditions:

$$\begin{cases} \$_{Tj} \circ \$_{Oi} = 0 \ \ (j = 1, 2, 3, j \neq i) \\ \$_{Ck} \circ \$_{Oi} = 0 \ \ (k = 1, 2, 3, 4, 5) \\ l^2 + m^2 + n^2 = 1. \end{cases} \tag{22}$$

For a detailed calculation process and rigorous mathematical proof of the above expression, literature is recommended in the introduction section. In brief, the input twist screw, the transmission wrench twist and the output twist screw of the manipulator can be obtained for given structural parameters and pose of the PM, respectively, which will be employed in the performance analysis in terms of the motion-force transmission in the subsequent section.

4.2 Motion-force transmission performance indices

Motion-force transmission performance index is one of the main methods for evaluating the performance of the lower mobility PM. By analyzing the motion-force transmission performance, the parameters of the PM can be optimized so that the mechanism has better working performance.

1) The input transmission performance index of the i-th chain can be expressed mathematically as

$$\lambda_i = \frac{|\$_{Ii} \circ \$_{Ti}|}{|\$_{Ii} \circ \$_{Ti}|_{\max}} \quad (i = 1, 2, 3, 4) \tag{23}$$

where λ_i denotes the ratio between the instantaneous power coefficient $\left|\$_{Ii} \circ \$_{Ti}\right|$ and the potential maximum power coefficient $\left|\$_{Ii} \circ \$_{Ti}\right|_{\max}$.

For the PM, the minimum value λ_i of the input transmission power can be used as an index to evaluate the input transmission performance of the whole PM, i.e.,

$$\lambda = \min(\lambda_i)\,. \tag{24}$$

2) Similarly, the output transmission index of the i-th chain can be defined as

$$\eta_i = \frac{|\$_{Ti} \circ \$_{Oi}|}{|\$_{Ti} \circ \$_{Oi}|_{\max}} (i = 1, 2, 3, 4). \tag{25}$$

Therefore, the key issue of (25) is converted to the determination of $\left|\$_{Ti} \circ \$_{Oi}\right|_{\max}$, i.e., the determination of h_i and $d_{\max}$ in the equation $\left|\$_{Ti} \circ \$_{Oi}\right|_{\max} = \sqrt{{h_i}^2 + d_{\max}^2}$, where h_i denotes the pitch of $\$_{Oi}$, and $d_{\max}$ represents the potential maximal length of the common perpendicular between the axes of the screw $\$_{Ti}$ and $\$_{Oi}$, respectively.

According to the characteristic point method[45], the transmission force screw $\$_{Ti}$ always passes through the central point of the joints of the moving platform, and the maximum value $d_{\max}$ between the feature point P and output twist screw $\$_{Oi}$ can be expressed by the equation as follows:

$$d_{\max} = |\boldsymbol{s}_{oi} \times \boldsymbol{l}_i| \tag{26}$$

where $\boldsymbol{s}_{oi}$ denotes the unit vector along the axis of the twist screw $\$_{Oi}$, and $\boldsymbol{l}_i$ denotes an arbitrary point vector from the feature point P to the axis. Therefore, the kernel issue of (26) is to determine a point Q in the twist screw $\$_{Oi}$. However, the method of determining the key point Q is not described in detail in the literature[46]. Therefore, in this paper, the concise concept and the simple method of determining the key point Q is proposed, which is not only to enrich the previous theory for determining the characteristic length, but also to improve the algorithm for seeking the maximal distance $d_{\max}$. Here, the key point Q was defined unambiguously, and there is no need to determine the two characteristic points, although a lot of researchers stated it was more or less the same as the characteristic point or application point proposed by Liu et al.[47, 48]

Without loss of generality, the generalized output twist screw is set as a unit screw, and its coordinate form in Plücker can be expressed as

$$\$_O = (s, s_0) = (s, r \times s + h \cdot s) \tag{27}$$

where s is a unit vector directing along the axis of output twist screw $\$_O$, s_0 is the moment of line between the vector s and the coordinate origin, respectively. Moreover, r denotes the position vector pointing from an arbitrary point on the screw axis to the origin of the reference coordinate system, the vector $r \times s$ defines the moment of the screw axis with respect to the origin of the reference coordinate system, and h represents the pitch of the screw. By taking the dot product of two vectors, we can obtain

$$s \cdot (r \times s + hs) = hs \cdot s. \tag{28}$$

Then, the pitch h can be expressed as

$$h = \frac{s \cdot s_0}{s_0 \cdot s_0}. \tag{29}$$

By taking the cross product of the vector s and the pitch s_0, we can get

$$s \times (r \times s + hs) = r - s\,(s \cdot r)\,. \tag{30}$$

If the vector s is perpendicular to radius vector r, then $s \cdot r = 0$.

Then, (30) can be further expressed as

$$s \times (r \times s + hs) = r. \tag{31}$$

Therefore, if given the twist screw $\$_O$, we can obtain key point Q through the radius vector r that is perpendicular to the vector direction of the output twist screw, l can be obtained, and then the maximum value $d_{\max}$ can be obtained as well, as is shown in Fig. 3.

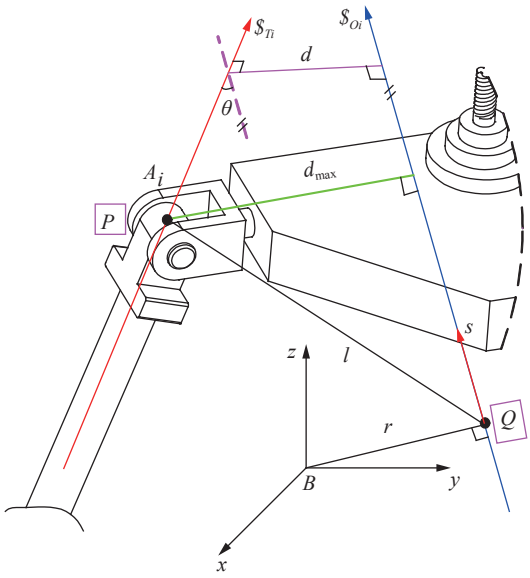

Fig. 3 $\$_{Oi}$, $\$_{Ti}$, $d_{\max}$ and l of the PM

In summary, just like the input transmission index, we treat the minimum value η_i of all the chains as the output transmission performance of the whole PM, so the output transmission performance of the PM can be defined as

$$\eta = \min\,(\eta_i)\,. \tag{32}$$

Obviously, the closer λ or η is to 1, the better the motion-force transmission performance is, while when a certain index value is very small or close to zero, then the motion-force transmission performance from the input chain to output terminal is very poor, even unable to complete the transmit ability. Therefore, it is necessary and reasonable to take the whole manipulator, rather than a single chain, into account when evaluating the motion force transmission performance of the manipulator. So the local transmission index (LTI) can be defined as

$$\chi = \min\,(\lambda, \eta)\,. \tag{33}$$

It is not hard to see that the value of χ varies from zero to one, the physical meaning is consistent, and is a performance evaluation index that is independent of the coordinate system, which can be used to reveal the influence rules between the structural parameters and the performance index, the larger is the value χ, the better is the motion force transmission performance of the mechanism under the instantaneous orientation configuration.

Considering the value χ varied with the configuration, the mean value of the local transmission index in the task workspace can be hereby utilized as a global transmission index (GTI) to evaluate the performance of the manipulator, which is expressed numerically as

$$\bar{\chi} = \frac{\int_{W_t} \chi \mathrm{d}W_t}{\int_{W_t} \mathrm{d}W_t}. \tag{34}$$

According to the concept of the pressure angle, the good transmission workspace (GTW) can be defined as a region that the local transmission index value is greater than 0.7, and the motion-force transmission performance index of all the pose configurations in this wide range region is good, and it is far away from the singularity position in general.

$$\chi_{GTW} = \chi \geq 0.7. \tag{35}$$

5 Workspace analysis

Workspace is the working region of the end effector of the PM, and it is an important performance index when designing the mechanism parameters. The main analytical methods include the analytic method and the numerical method. In this paper, the numerical search method is utilized to calculate the workspace.

5.1 Constraint conditions

In the actual task of the PM tool, the following limitations should be considered:

1) Limitations of the actuated joints s_i:

$$s_{\min} \leq s_i \leq s_{\max} \tag{36}$$

where $s_{\min}$ and $s_{\max}$ represent the minimum and maximum linear displacement of the i-th actuator respectively. Here, $s_{\min}$ =0 and $s_{\max}$=650 mm.

2) Limitation of redundantly actuated joint q_4:

$$q_{\min} \leq q_4 \leq q_{\max} \tag{37}$$

where $q_{\min}$ and $q_{\max}$ represent the minimum and maximum displacement of the second stage active joint of the third limb, respectively.

3) Joint angle constraints:

a) The rotation angle R_{2i} of the rotation joint R should be satisfied as

$$R_{2\min} \leq R_{2i} = a\cos\left(\frac{\boldsymbol{s}_{1i}\cdot\boldsymbol{l}_{i0}}{|\boldsymbol{s}_{1i}|\,|\boldsymbol{l}_{i0}|}\right) \leq R_{2\max} \tag{38}$$

where $R_{2\min}$ and $R_{2\max}$ represent the minimum and maximum limit angles of the rotation joint R of the i-th limb, respectively. Here, $R_{2\min}=0$ and $R_{2\max}=\dfrac{\pi}{6}$.

b) The rotation angle R_{3i} of the first revolute axis of the Hooke joint is

$$R_{3\,\min} \leq R_{3i} = a\cos\left(\frac{\boldsymbol{s}_{4i}\cdot\boldsymbol{l}_{i0}}{|\boldsymbol{s}_{4i}|\,|\boldsymbol{l}_{i0}|}\right) \leq R_{3\,\max} \tag{39}$$

where $R_{3\min}$ and $R_{3\max}$ represent the minimum and maximum angles of the first revolute axis of the Hooke joint of the i-th limb, respectively. Here $R_{3\min}=\dfrac{\pi}{6}$ and $R_{3\max}=\pi$.

c) The rotation angle R_{53} of the second revolute axis of the compound spherical joint should be satisfied as

$$R_{4\min} \leq R_{53} = a\cos\left(\frac{\boldsymbol{s}_{6i}\cdot\boldsymbol{l}_{i0}}{|\boldsymbol{s}_{6i}|\,|\boldsymbol{l}_{i0}|}\right) \leq R_{4\max} \tag{40}$$

where $R_{4\min}$ and $R_{4\max}$ represent the minimum and maximum angles of the second revolute axis of the compound spherical joint, respectively. Here, $R_{4\min}=\dfrac{\pi}{9}$ and $R_{4\max}=\pi$.

5.2 Boundary search process

According to the structural parameters of the given PM, a discrete boundary searching method is developed to calculate and visualize the reachable workspace. The searching method is directly based on the calculation of inverse kinematics and the aforementioned constraint conditions. The workspace can be carried out by the following steps:

1) The center of the moving platform moves a small subspace Δz along z translational direction.

2) Given the minimum value z of the center of moving platform, let the moving platform rotate, and the orientation parameters φ and ϕ are searched from initial value to the maximum, if the points meet the inverse kinematics and constraint conditions, and then the points will be recorded and saved.

3) z will increase Δz, and repeat the step 2) until the condition $z{=}z_{\max.}$

4) A three dimensional array can be obtained, and the workspace including the reachable workspace and task workspace of the manipulator will be generated by Matlab programming.

6 Numerical examples

In this section, the performance of the 2PRU-PRPS PM is discussed including the parasitic motions, the input transmission index, output transmission index, local transmission index, reachable workspace, task workspace and global transmission workspace. The architectural parameters are shown in Table 1 as below.

Table 1 Architecture parameters of the proposed PM

Parameter	Value	Parameter	Value
a (mm)	300	$\alpha(^\circ)$	[−80,80]
b (mm)	600	$\beta(^\circ)$	[−90, 90]
l_1 (mm)	1045	z (mm)	[1000, 1600]
l_2 (mm)	1045	φ	$[0, 2\pi]$
l_3 (mm)	[900, 1200]	ϕ	$[0, \frac{\pi}{2}]$

6.1 Parasitic motion

In kinematic analysis, parasitic motions, which are unexpected motions occurred on the constrained directions, should be identified first. Generally, the 1T2R PM not only has three main motions, but also three parasitic motions. This characteristic should be investigated in detail. Here, the redundantly actuated and overconstrained 2PRU-PRPS PM was no exception. According to (13), γ can be ignored. Here only parasitic motion along the y-axis direction is discussed. The simulation result of parasitic motion is obtained and the mapping relation atlas between $|y|$ and (φ,ϕ) is depicted in Fig. 4.

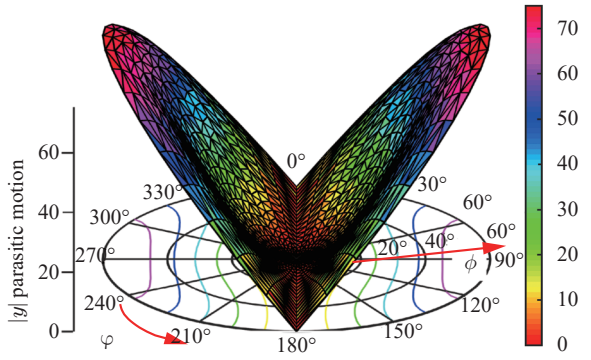

Fig. 4 Parasitic motion between $|y|$ and (φ,ϕ)

6.2 Motion-force transmission performance analysis

For a given PM, the performance will change with the variation of the manipulator configuration within its workspace. Once the transmission index is derived, it is desired to evaluate the transmission characteristics over the workspace. What's more, it is necessary to investigate the transmission performance at a specific configuration to have an insight into its transmission behaviour.

Figs. 5–7 show that influence rules of the redundantly actuated and active overconstrainted 2PRU-PRPS PM about the input transmission index, the output transmis-

sion index and the local transmission on (φ, ϕ) when l_3=1 150 mm and z=1 300 mm. Figs. 6 and 7 show that the middle region has a better kinematic performance, and the atlas of Figs. 5–7 show that the distribution of the transmission index in workspace is symmetrical about the x-axis due to structural features and the value will be worsened when it comes near the workspace boundary.

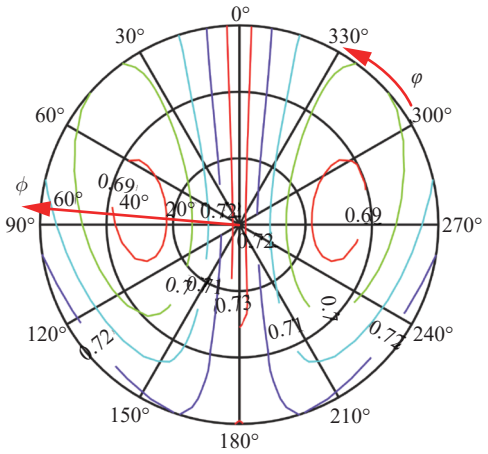

Fig. 5 Input transmission index

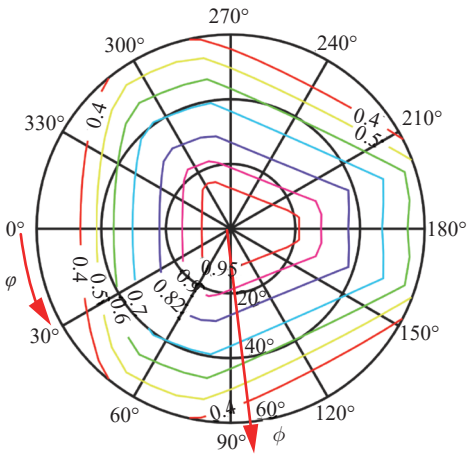

Fig. 6 Output transmission index

Fig. 8 shows that the curve line between the structural inclination angle θ and the input transmission index, output transmission index and local transmission index can be visually seen when the moving platform located $(30°, 30°, 1\,180)$. It can be clearly seen from Fig. 8 that the input transmission index is smaller than the output transmission index when $20° \leq \theta \leq 40°$, and the output transmission index is smaller than the input transmission index when $40° \leq \theta \leq 70°$.

Figs. 9 and 10 show two local transmission performance index comparisons with overconstrained PMs, wherein 2PRU-PRS is a passive overconstrained PM, and the proposed 2PRU-PRPS is called an active overconstrained PM. Fig. 9 indicates that the local transmission index changes with (φ, ϕ), when l_3=950 mm, and

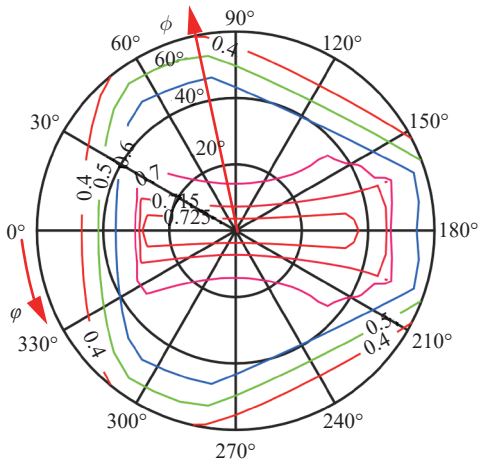

Fig. 7 Local transmission index

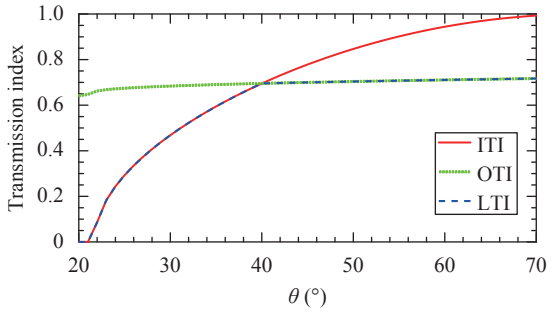

Fig. 8 Influence rule of structural inclination angle on the performance index

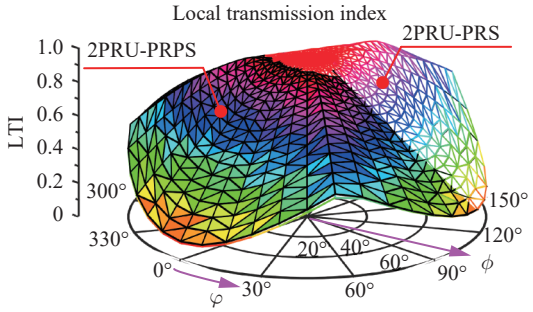

Fig. 9 LTI refer to (φ, ϕ) when $l_3 = 950$, $z = 1\,250$

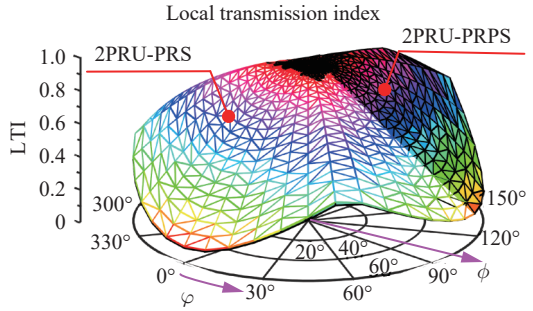

Fig. 10 LTI refer to (φ, ϕ) when $l_3 = 1\,150$, $z = 1\,250$

$z=1\,250$ mm. Fig. 10 indicates that the local transmission index changes with (φ, ϕ), when $l_3=1\,150$ mm, and $z=1\,250$ mm. The higher LTI is reached at the home position, and LTI is also decreased by rotation with ϕ.

We can see from Fig. 9, the local transmission index of the 2PRU-PRPS PM is higher than the 2PRU-PRS PM when $0° \leq \varphi \leq 120°$ and $120° \leq \varphi \leq 360°$. While we can see from Fig. 10, the local transmission index of the 2PRU-PRPS PM compared with passive overconstrained 2PRU-PRS PM is much higher. The redundant actuation and active overconstrained 2PRU-PRPS PM can change the extension or shorten the redundant chain to achieve the switch of the working mode, so that the PM can always maintain the best motion-force transmission performance.

6.3 Workspace performance analysis

To illustrate the analytic process of the workspace including reachable workspace and task workspace, the novel PM proposed has been taken as an example. By adopting the aforementioned numerical searching method, the reachable workspace and task workspace of the redundantly actuated and overconstrained PM are generated as shown in Fig. 11, in other words, the machine tool will possess a workspace, encasing a specified task workspace. The results show that the manipulator can translate 900 mm to 1 600 mm along the z axis, rotate 0° to 360° about φ, and rotate 0° to 90° about ϕ.

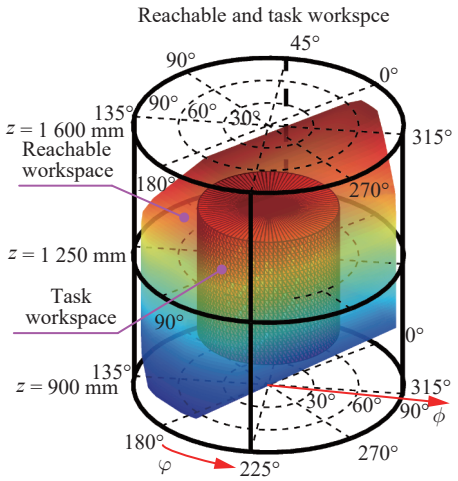

Fig. 11 Reachable and task workspace

The reachable workspace of the proposed PM and the overconstrained 2PRU-PRS PM, with the same degree of freedom, is illustrated in Fig. 12. To facilitate analysis, the same search space is used for comparison with the overconstrained 2PRU-PRS and the proposed PM. The results indicate that the proposed manipulator has a redundancy actuation chain to accomplish better orientation capability in contrast to the 2PRU-PRS PM. And it is easier to develop the manipulator into practical application.

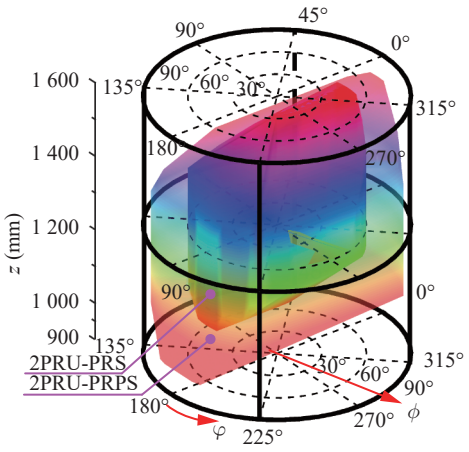

Fig. 12 Workspace comparison of two PMs

Fig. 13 demonstrated the good transmission workspace based on the constraint conditions that the kinematic inverse position, limitation of actuations, joint angle constraints, non-singularity and geometric constraints, and local motion-force transmission index LTI is greater than 0.7. In the trajectory planning of the PM, the manipulator should be working in the optimum working region as soon as possible, so that the manipulator has better kinematics performance, so as to improve the motion accuracy and control accuracy of the manipulator.

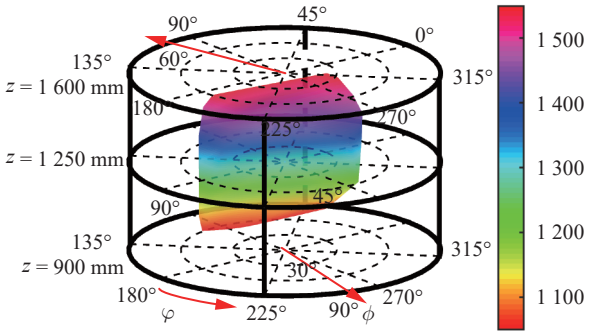

Fig. 13 Good transmission workspace

7 Conclusions

In this paper, the kinematics analysis and performance evaluation of the proposed PM, which can be constructed as a 5-axis hybrid machine tool to accomplish high speed machining of a large complex component in the aerospace field, are investigated in detail, and the following conclusions are obtained

1) The mobility of the proposed redundantly actuated and overconstrained 2PRU-PRPS PM has been analysed in detail based on the screw theory. The inverse kinematic position and parasitic motion of the derived

PM have been sequentially analysed, and the relationship between the *Z-Y-X* Euler angle and the T-T angle is briefly expressed.

2) By using the screw theory, the input transmission index, the output transmission index, the local transmission index, the global transmission index and the good transmission workspace are introduced. Most importantly, a simple calculation method of potential maximum transmission power is straightforwardly identified, and the maximum virtual power coefficient can be obtained expediently via this approach.

3) The motion-force transmission indices and workspace can serve as an alternative for the description of the manipulator performance. Compared with the overstrained 2PRU-PRS PM, the corresponding results illustrate that the redundancy actuation PM can effectively increase the workspace and potentially improve its motion-force transmissibility characteristics, which lays a theoretical foundation for the stiffness analysis and optimal design of the PM in the future work.

Acknowledgments

This work was supported by the Fundamental Research Funds for the Central Universities (Nos. 2018JBZ007, 2018YJS136 and 2017YJS158), China Scholarship Council (CSC) (No. 201807090079), and National Natural Science Foundation of China (NSFC) (No. 51675037).

References

[1] X. Chen, X. J. Liu, F. G. Xie, T. Sun. A comparison study on motion/force transmissibility of two typical 3-DOF parallel manipulators: The sprint Z3 and A3 tool heads. *International Journal of Advanced Robotic Systems*, vol. 11, no. 1, pp. 1–11, 2014. DOI: 10.5772/57458.

[2] Y. Y. Wang, H. T. Liu, T. Huang, D. G. Chetwynd. Stiffness modeling of the Tricept robot using the overall Jacobian matrix. *Journal of Mechanisms and Robotics*, vol. 1, no. 2, Article number 021002, 2009. DOI: 10.1115/5.1.3046131.

[3] J. Zhang, Y. Q. Zhao, Y. Jin. Elastodynamic modeling and analysis for an Exechon parallel kinematic machine. *Journal of Manufacturing Science and Engineering*, vol. 138, no. 3, Article number 031011, 2016. DOI: 10.1115/5. 5.1.4030938.

[4] J. Brinker, B. Corves, Y. Takeda. Kinematic performance evaluation of high-speed Delta parallel robots based on motion/force transmission indices. *Mechanism and Machine Theory*, vol. 125, pp. 111–125, 2018. DOI: 10.1016/j.mechmachtheory.2017.11.029.

[5] B. Hu, Z. Huang. Kinetostatic model of overconstrained lower mobility parallel manipulators. *Nonlinear Dynamics*, vol. 86, no. 1, pp. 309–322, 2016. DOI: 10.1007/s11071-016-2890-2.

[6] M. Hu, J. S. Shi. The kinematic analyses of the 3-DOF parallel machine tools. *International Journal of Automation and Computing*, vol. 8, no. 1, pp. 107–111, 2011. DOI: 10.1007/s11633-010-0561-1.

[7] A. Pashkevich, D. Chablat, P. Wenger. Stiffness analysis of 3-d.o.f overconstrained translational parallel manipulators. In *Proceedings of IEEE International Conference on Robotics and Automation*, Pasadena, USA, pp. 1562–1567, 2008. DOI: 10.1109/ROBOT.2008.4543424.

[8] H. Zhang, H. Fang, B. Jiang. Dynamic performance evaluation of a redundantly actuated and over-constrained parallel manipulator. *International Journal of Automation and Computing*, Online first, 2018. DOI: 10.1007/s11633-018-1147-6.

[9] Y. G. Li, H. T. Liu, X. M. Zhao, T. Huang, D. G. Chetwynd. Design of a 3-DOF PKM module for large structural component machining. *Mechanism and Machine Theory*, vol. 45, no. 6, pp. 941–954, 2010. DOI: 10.1016/j.mechmachtheory.2010.01.008.

[10] X. Kong, C. M. Gosselin. Type synthesis of three-DOF upequivalent parallel manipulators using a virtual-chain approach. *Advances in Robot Kinematics*, J. Lennarcic, B. Roth, Eds., Dordrecht, Netherlands: Springer, pp. 123–132, 2006. DOI: 10.1007/978-1-4020-4941-5_14.

[11] Q. C. Li, J. M. Herve. Type synthesis of 3-DOF RPR-equivalent parallel mechanisms. *IEEE Transactions on Robotics*, vol. 30, no. 6, pp. 1333–1343, 2014. DOI: 10.1109/TRO.2014.2344450.

[12] Q. C. Li, Z. Chen, Q. H. Chen, C. Y. Wu, Z. Huang. Structural condition for [PP]S parallel mechanism without parasitic motion. *Journal of Mechanical Engineering*, vol. 46, no. 15, pp. 31–35, 2010. DOI: 10.3901/JME.200.15.031. (in Chinese)

[13] L. P. Wang, H. Y. Xu, L. W. Guan. Optimal design of a 3-PUU parallel mechanism with 2R1T DOFs. *Mechanism and Machine Theory*, vol. 114, pp. 190–203, 2017. DOI: 10.1016/j.mechmachtheory.2017.03.008.

[14] X. L. Cui, X. G. Han, W. Y. Chen. Continuous stiffness modeling of 3-RPS parallel kinematic machine with special composite spherical joints. *Journal of Beijing University of Aeronautics and Astronautics*, vol. 36, no. 11, pp. 1275–1280, 2010. DOI: 10.13700/j.bh.1001-5965.2010.11.024. (in Chinese)

[15] B. Li, Y. M. Li, X. H. Zhao. Kinematics analysis of a novel over-constrained three degree-of-freedom spatial parallel manipulator. *Mechanism and Machine Theory*, vol. 104, pp. 222–233, 2016. DOI: 10.1016/j.mechmachtheory.2016.06.003.

[16] F. G. Xie, X. J. Liu, T. M. Li. A comparison study on the orientation capability and parasitic motions of two novel articulated tool heads with parallel kinematics. *Advances in Mechanical Engineering*, vol. 5, Article number 249103, 2013. DOI: 10.1155/2013/249103.

[17] A. Pashkevich, D. Chablat, P. Wenger. Stiffness analysis of overconstrained parallel manipulators. *Mechanism and Machine Theory*, vol. 44, no. 5, pp. 966–982, 2009. DOI: 10.1016/j.mechmachtheory.2008.05.017.

[18] H. B. Qu, Y. F. Fang, S. Guo. A new method for isotropic analysis of limited DOF parallel manipulators with terminal constraints. *Robotica*, vol. 29, no. 4, pp. 563–569, 2011. DOI: 10.1017/S0263574710000470.

[19] J. Denavit, R. S. Hartenbe, R. Razi, J. J. Uicker. Velocity, acceleration, and static-force analyses of spatial linkages.

Journal of Applied Mechanics, vol. 32, no. 4, pp. 903–910, 1965. DOI: 10.1115/1.3627334.

[20] K. Watanabe, H. Funabashi. Kinematic analysis of Stephenson six-link mechanisms: 2nd report, index of motion-transmission characteristics. *Bulletin of the JSME*, vol. 27, no. 234, pp. 2871–2878, 1984. DOI: 10.1299/jsme1958.27.2871.

[21] T. Yoshikawa. Manipulability of robotic mechanisms. *The International Journal of Robotics Research*, vol. 4, no. 2, pp. 3–9, 1985. DOI: 10.1177/027836498500400201.

[22] D. Wang, R. Fan, W. Y. Chen. Performance enhancement of a three-degree-of-freedom parallel tool head via actuation redundancy. *Mechanism and Machine Theory*, vol. 71, pp. 142–162, 2014. DOI: 10.1016/j.mechmachtheory.2013.09.006.

[23] J. P. Merlet. Jacobian, Manipulability, Condition Number and Accuracy of Parallel Robots. In *Proceedings of International Symposium on Robotics Research*, Springer, Hiroshima, Japan, pp. 175–184, 2007. DOI: 10.1007/978-3-540-48113-3_16.

[24] G. Pond, J. A. Carretero. Formulating Jacobian matrices for the dexterity analysis of parallel manipulators. *Mechanism and Machine Theory*, vol. 41, no. 12, pp. 1505–1519, 2006. DOI: 10.1016/j.mechmachtheory.2006.01.003.

[25] C. Gosselin, J. Angeles. A global performance index for the kinematic optimization of robotic manipulator. *Journal of Mechanical Design*, vol. 113, no. 3, pp. 220–226, 1991. DOI: 10.1115/1.2912772.

[26] R. S. Ball. *A Treatise on the Theory of Screws*, Cambridge, UK: Cambridge University Press, 1900.

[27] M. S. C. Yuan, F. Freudenstein, L. S. Woo. Kinematic analysis of spatial mechanisms by means of screw coordinates. Part 2-Analysis of spatial mechanisms. *Journal of Engineering for Industry*, vol. 91, no. 1, pp. 67–73, 1971. DOI: 10.1115/1.3427919.

[28] G. Sutherland, B. Roth. A transmission index for spatial mechanisms. *Journal of Engineering for Industry*, vol. 95, no. 2, pp. 589–597, 1973. DOI: 10.1115/1.3438195.

[29] M. J. Tsai, H. W. Lee. The transmissivity and manipulability of spatial mechanisms. *Journal of Mechanical Design*, vol. 116, no. 1, pp. 137–143, 1994. DOI: 10.1115/1.2919337.

[30] M. J. Tsai, H. W. Lee. Generalized evaluation for the transmission performance of mechanisms. *Mechanism and Machine Theory*, vol. 29, no. 4, pp. 607–618, 1994. DOI: 10.1016/0094-114X(94)90098-1.

[31] Y. Takeda, H. Funabashi. Motion transmissibility of In-Parallel actuated manipulators. *JSME International Journal Series C*, vol. 38, no. 4, pp. 749–755, 1995. DOI: 10.1299/jsmec1993.38.749.

[32] C. Chen, J. Angeles. Generalized transmission index and transmission quality for spatial linkages. *Mechanism and Machine Theory*, vol. 42, no. 9, pp. 1225–1237, 2007. DOI: 10.1016/j.mechmachtheory.2006.08.001.

[33] F. G. Xie, X. J. Liu, J. S. Wang. Performance evaluation of redundant parallel manipulators assimilating motion/force transmissibility. *International Journal of Advanced Robotic Systems*, vol. 8, no. 5, pp. 113–124, 2011. DOI: 10.5772/50904.

[34] X. Chen, F. G. Xie, X. J. Liu. Singularity analysis of the planar 3-RRR parallel manipulator considering the motion/force transmissibility. In *Proceedings of the 5th International Conference on Intelligent Robotics and Applications*, Springer, Montreal, Canada, pp. 250–260, 2012. DOI: 10.1007/978-3-642-33509-9_24.

[35] T. Huang, M. X. Wang, S. F. Yang, T. Sun, D. G. Chetwynd, F. G. Xie. Force/motion transmissibility analysis of six degree of freedom parallel mechanisms. *Journal of Mechanisms and Robotics*, vol. 6, no. 3, Article number 031010, 2014. DOI: 10.1115/1.4026631.

[36] H. T. Liu, M. X. Wang, T. Huang, D. G. Chetwynd, A. Kecskeméthy. A dual space approach for force/motion transmissibility analysis of lower mobility parallel manipulators. *Journal of Mechanisms and Robotics*, vol. 7, no. 3, Article number 034504, 2015. DOI: 10.1115/1.4030371.

[37] Z. Z. Chi, D. Zhang, L. Xia, Z. Gao. Multi-objective optimization of stiffness and workspace for a parallel kinematic machine. *International Journal of Mechanics and Materials in Design*, vol. 9, no. 3, pp. 281–293, 2013. DOI: 10.1007/s10999-013-9219-9.

[38] M. A. Hosseini, H. R. M. Daniali, H. D. Taghirad. Dexterous workspace optimization of a Tricept parallel manipulator. *Advanced Robotics*, no. 13–14, pp. 1697–1712, 2011. DOI: 10.1163/016918611X584640.

[39] G. Pond, J. A. Carretero. Quantitative dexterous workspace comparison of parallel manipulators. *Mechanism and Machine Theory*, vol. 42, no. 10, pp. 1388–1400, 2007. DOI: 10.1016/j.mechmachtheory.2006.10.004.

[40] S. Herrero, C. Pinto, O. Altuzarra, M. Diez. Workspace study of the 2PRU-1PRS parallel manipulator. In *Proceedings of the 14th IFToMM World Congress in Mechanism and Machine Science*, Taipei, China, 2015. DOI: 10.6567/IFToMM.14TH.WC.OS13.063.

[41] J. X. Fu, F. Gao. Optimal design of a 3-Leg 6-DOF parallel manipulator for a specific workspace. *Chinese Journal of Mechanical Engineering*, vol. 29, no. 4, pp. 659–668, 2016. DOI: 10.3901/CJME.2016.0121.011.

[42] H. Q. Zhang, H. R. Fang, Y. F. Fang, B. S, Jiang. Workspace analysis of a hybrid kinematic machine tool with high rotational applications. *Mathematical Problems in Engineering*, Article number 2607497, 2018. DOI: 10.1155/2018/2607497.

[43] M. Mazare, M. Taghizadeh, M. R. Najafi. Kinematic analysis and design of a 3-DOF translational parallel robot. *International Journal of Automation and Computing*, vol. 14, no. 4, pp. 432–441, 2017. DOI: 10.1007/s11633-017-1066-y.

[44] X. J. Liu, C. Wu, J. S. Wang, I. BONEV. Attitude description method of [PP]S type parallel robotic mechanisms. *Chinese Journal of Mechanical Engineering*, vol. 44, no. 10, pp. 19–23, 2008. DOI: 10.3321/j.issn:0577-6686.2008.10.003. (in Chinese)

[45] Q. C. Li, N. B. Zhang, F. B. Wang. New indices for optimal design of redundantly actuated parallel manipulators. *Journal of Mechanisms and Robotics*, vol. 9, no. 1, pp. 011007, 2016. DOI: 10.1115/1.4035126.

[46] J. S. Wang, C. Wu, X. J. Liu. Performance evaluation of parallel manipulators: Motion/force transmissibility and its index. *Mechanism and Machine Theory*, vol. 45, no. 10, pp. 1462–1476, 2010. DOI: 10.1016/j.mechmachtheory.2010.05.001.

[47] H. Liu, T. Huang, A. Kecskemethy, D. G. Chetwynd. Force/Motion/Stiffness transmissibility analyses of redundantly actuated and overconstrained parallel manipulators. In *Proceedings of the 14th IFToMM World Congress in Mechanism and Machine Science*, Taipei, China, 2015. DOI: 10.6567/IFToMM.14TH.WC.OS13.013.

[48] H. Liu, T. Huang, Kecskeméthy A, D. G. Chetwynd. A generalized approach for computing the transmission index of parallel mechanisms. *Mechanism and Machine Theory*, vol. 74, pp. 245–256, 2014. DOI: 10.1016/j.mechmachtheory.2013.12.012.

Hai-Qiang Zhang received the B. Sc. degree in mechanical design and theories from Yantai University, China in 2012, and the M. Sc. degree in mechanical engineering from Hebei University of Engineering, China in 2015. He is a Ph. D. degree candidate in mechanical, electronic and control engineering at Beijing Jiaotong University, China. In 2018, he receive the China Scholarship Council (CSC) Founding to York University, Canada as a joint Ph. D. student.

His research interests include robotics in computer integrated manufacturing, parallel kinematics machine tool, redundancy actuation robots, over-constrained parallel manipulators, and multi-objective optimization design.

E-mail: hqzhang@bjtu.edu.cn

ORCID iD: 0000-0003-4421-5671

Hai-Rong Fang received the B. Sc. degree in mechanical engineering from Nanjing University of Science and Technology, China in 1990, the M. Sc. degree in mechanical engineering from Sichuan University, China in 1996, and the Ph. D. degree in mechanical engineering from Beijing Jiaotong University, China in 2005. She worked as an associate professor in Department of Engineering Mechanics, Beijing Jiaotong University, China, from 2003 to 2011. She is a professor at School of Mechanical Engineering from 2011 and director of Robotics Research Center.

Her research interests include the parallel mechanisms, digital control, robotics and automation, machine tool equipment.

E-mail: hrfang@bjtu.edu.cn (Corresponding author)

ORCID iD: 0000-0001-7938-4737

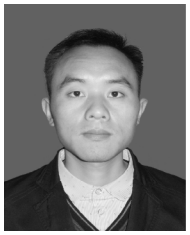

Bing-Shan Jiang received the B. Sc. degree in mechanical electronic engineering from Liaoning Technical University, China in 2015, and the M. Sc. degree in mechanical engineering from Liaoning Technical University, China in 2017. He is currently a Ph. D. degree candidate in mechanical, electronic and control engineering, Beijing Jiaotong University, China.

His research interests include synthesis, kinematics, dynamics and control of parallel robots.

E-mail: 17116381@bjtu.edu.cn